



THE BURSTY STAR FORMATION HISTORIES OF LOW-MASS GALAXIES AT $0.4 < z < 1$ REVEALED BY STAR FORMATION RATES MEASURED FROM $H\beta$ AND FUV

YICHENG GUO¹, MARC RAFELSKI^{2,15,16}, S. M. FABER¹, DAVID C. KOO¹, MARK R. KRUMHOLZ^{1,3}, JONATHAN R. TRUMP^{4,17}, S. P. WILLNER⁵, RICARDO AMORÍN⁶, GUILLERMO BARRO^{1,7}, ERIC F. BELL⁸, JONATHAN P. GARDNER², ERIC GAWISER⁹, NIMISH P. HATHI¹⁰, ANTON M. KOEKEMOER¹¹, CAMILLA PACIFICI^{2,15}, PABLO G. PÉREZ-GONZÁLEZ¹², SWARA RAVINDRANATH¹¹, NAVEEN REDDY¹³, HARRY I. TEPLITZ¹⁴, AND HASSEN YESUF¹

¹UCO/Lick Observatory, Department of Astronomy and Astrophysics, University of California, Santa Cruz, CA, USA; ycguo@ucolick.org

²Goddard Space Flight Center, Code 665, Greenbelt, MD, USA

³Research School of Astronomy, and Astrophysics, Australian National University, Canberra, ACT 2611, Australia

⁴Department of Astronomy and Astrophysics and Institute for Gravitation and the Cosmos, Pennsylvania State University, University Park, PA, USA

⁵Harvard-Smithsonian Center for Astrophysics, Cambridge, MA, USA

⁶INAF-Osservatorio Astronomico di Roma, Monte Porzio Catone, Italy

⁷Department of Astronomy, University of California, Berkeley, CA, USA

⁸Department of Astronomy, University of Michigan, Ann Arbor, MI, USA

⁹Department of Physics and Astronomy, Rutgers University, New Brunswick, NJ, USA

¹⁰Aix Marseille Université, CNRS, LAM (Laboratoire d'Astrophysique de Marseille) UMR 7326, Marseille, France

¹¹Space Telescope Science Institute, Baltimore, MD, USA

¹²Departamento de Astrofísica, Facultad de CC. Físicas, Universidad Complutense de Madrid, E-28040 Madrid, Spain

¹³Department of Physics and Astronomy, University of California, Riverside, CA, USA

¹⁴Infrared Processing and Analysis Center, Caltech, Pasadena, CA 91125, USA

Received 2016 April 15; revised 2016 September 26; accepted 2016 October 2; published 2016 December 6

ABSTRACT

We investigate the burstiness of star formation histories (SFHs) of galaxies at $0.4 < z < 1$ by using the ratio of star formation rates (SFRs) measured from $H\beta$ and FUV (1500 Å) ($H\beta$ -to-FUV ratio). Our sample contains 164 galaxies down to stellar mass (M_*) of $10^{8.5} M_\odot$ in the CANDELS GOODS-N region, where Team Keck Redshift Survey Keck/DEIMOS spectroscopy and *Hubble Space Telescope*/WFC3 F275W images from CANDELS and Hubble Deep UV Legacy Survey are available. When the ratio of $H\beta$ - and FUV-derived SFRs is measured, dust extinction correction is negligible (except for very dusty galaxies) with the Calzetti attenuation curve. The $H\beta$ -to-FUV ratio of our sample increases with M_* and SFR. The median ratio is ~ 0.7 at $M_* \sim 10^{8.5} M_\odot$ (or $\text{SFR} \sim 0.5 M_\odot \text{ yr}^{-1}$) and increases to ~ 1 at $M_* \sim 10^{10} M_\odot$ (or $\text{SFR} \sim 10 M_\odot \text{ yr}^{-1}$). At $M_* < 10^{9.5} M_\odot$, our median $H\beta$ -to-FUV ratio is lower than that of local galaxies at the same M_* , implying a redshift evolution. Bursty SFH on a timescale of a few tens of megayears on galactic scales provides a plausible explanation for our results, and the importance of the burstiness increases as M_* decreases. Due to sample selection effects, our $H\beta$ -to-FUV ratio may be an upper limit of the true value of a complete sample, which strengthens our conclusions. Other models, e.g., non-universal initial mass function or stochastic star formation on star cluster scales, are unable to plausibly explain our results.

Key words: galaxies: dwarf – galaxies: evolution – galaxies: formation – galaxies: fundamental parameters – galaxies: starburst – galaxies: star formation

1. INTRODUCTION

The star formation histories (SFHs) of galaxies with stellar masses (M_*) lower than $10^9 M_\odot$ (low-mass galaxies or dwarf galaxies) are expected to be bursty. In such galaxies, supernova feedback following an intense star formation (SF) episode can quickly heat and expel gas from them, resulting in a temporary quenching of SF. New gas accretion and recycling of the expelled gas then induce new SF. Therefore, the SFHs of dwarf galaxies in many models are characterized by frequent bursts of SF and subsequent quick quenches on a timescale of a few or tens of megayears (e.g., Hopkins et al. 2014; Shen et al. 2014; Sparre et al. 2015).

Observationally, in their landmark paper, Searle et al. (1973) tentatively concluded, by using broadband colors, that the bluest (and dwarf) galaxies undergo “intermittent and unusually intense bursts of SF.” The ratio of star formation rates

(SFRs) measured from nebular emission lines and ultraviolet (UV) continuum provides a more direct tool than broadband colors to explore the burstiness of galaxy SFHs. Balmer line emission arises from the recombination of gas ionized by O-stars, which have lifetimes of only a few megayears. Thus, $H\alpha$ and $H\beta$ emissions trace SFR over a timescale of a few megayears. On the other hand, UV photons come from both O- and B-stars, which last for ~ 100 Myr. Therefore, traces SFRs over that timescale. As a result, a galaxy with an SFH that forms a significant fraction of its stars in bursts separated by ~ 5 – 100 Myr will spend short amounts of time with very high $H\alpha$ and $H\beta$ luminosities followed by long periods of low $H\alpha$ and $H\beta$ luminosities. The time variation of their FUV luminosities is much smoother. This effect does not alter the average luminosity—in comparison to galaxies with steady SFH of the same averaged value, a sample of bursty galaxies will still have the same mean FUV, $H\alpha$, and $H\beta$ luminosity—but it can alter the distribution, median, and mean values of the $H\alpha$ (or $H\beta$)-to-FUV ratio (Iglesias-Páramo et al. 2004; Fumagalli et al. 2011; da Silva et al. 2012, 2014; Weisz et al. 2012).

¹⁵ NASA Postdoctoral Program Fellow.

¹⁶ Current Address: Space Telescope Science Institute, Baltimore, MD, USA.

¹⁷ Hubble Fellow.

Thus, a measurement of this distribution or its moments can be a sensitive diagnostic of the SFH with the distribution of ratios depending on the intensity, duration, and separation of the bursts.

In the local universe, a number of authors have reported $H\alpha$ -to-FUV SFR ratios lower than unity for low-mass (and hence low-SFR) or dwarf galaxies (e.g., Sullivan et al. 2000; Bell & de Jong 2001; Boselli et al. 2009; Lee et al. 2009; Meurer et al. 2009; Weisz et al. 2012). The effect becomes noticeable for SFRs below $\sim 0.1 M_{\odot} \text{ yr}^{-1}$ and is absent in galaxies with higher SFRs. For a sample of galaxies, an average $H\alpha$ -to-FUV ratio lower than unity indicates that these galaxies are preferentially observed during their subsequent quenching following SF bursts.

Besides the bursty SFHs on galactic-wide scales, two other possibilities are often used to explain the observed lower-than-unity $H\alpha$ -to-FUV ratios: non-universal initial mass function (IMF) and stochastic SF on small (star or star cluster) scales. Non-universal IMF theories assume that the IMFs of galaxies depend on the properties of galaxies. One particular scenario, the integrated galactic initial mass function (IGIMF), predicts that the actual IMF is steeper than the canonical IMF and steepens with the decrease of the total SFR of galaxies (Weidner & Kroupa 2005; Pflamm-Altenburg et al. 2007, 2009; Weidner et al. 2011). This scenario assumes that (1) all stars form in clusters (e.g., Pflamm-Altenburg et al. 2007); (2) the cluster mass function is a power law; (3) the mass of the most massive star cluster (i.e., the truncation mass of the power law) is a function of the total SFR of a galaxy; and (4) the mass of the most massive star in a star cluster is a function of the mass of the cluster. As a result, the chance of forming a massive star in low-SFR galaxies is lower than in high-SFR galaxies. Consequently, low-SFR galaxies have steeper IMFs than high-SFR galaxies. Due to the lack of massive stars to ionize hydrogen, low-SFR galaxies, therefore, have lower $H\alpha$ -to-FUV ratio. Lee et al. (2009) found that the IGIMF model is able to account for the observed $H\alpha$ -to-FUV ratio in their Local Volume galaxy sample, but they also pointed out that a critical test of the IGIMF model would be the scatter of the $H\alpha$ -to-FUV ratio. Fumagalli et al. (2011) and Weisz et al. (2012, W12) compared the IGIMF model to their samples and found that the scatter predicted by IGIMF is not compatible with observations. In addition, observations of individual low-mass star clusters have failed to detect the deficiency in $H\alpha$ predicted by IGIMF models, and appear fully consistent with a universal, randomly sampled IMF (Andrews et al. 2013, 2014). While Andrews et al. (2013, 2014) were testing the mass of the most massive star in a star cluster (i.e., Assumption (4) listed above), Pflamm-Altenburg et al. (2013) tested Assumption (3)—the mass of the most massive star cluster—and found that the masses of the most massive young star clusters in M33 decrease with increasing galactocentric radius, supporting a non-universal truncation mass of the cluster mass function. Weidner et al. (2014) showed that some weaker versions of the IGIMF hypothesis (e.g., Weidner & Kroupa 2006) remain consistent with the Andrews et al. data, but the fact that the observations are also consistent with a universal IMF implies that they also provide no support for the hypothesis of non-universality.

Stochastic SF on small scales (e.g., Cerviño & Valls-Gabaud 2003; Cerviño & Luridiana 2004; Fumagalli et al. 2011; Eldridge 2012; da Silva et al. 2012; Cerviño 2013)

can also produce low $H\alpha$ -to-FUV ratio for low-SFR galaxies. Sometimes, bursty SFH is also considered as a stochastic process, but in this paper we use the following distinction: burstiness is caused by phenomena on galaxy scales (e.g., feedback, gas accretion, and merger, etc.), while stochasticity occurs on star or star cluster scale. The stochasticity considered in our paper is the stochastic sampling of IMFs and SFHs. Even for a universal IMF, when the SFR is low, the IMF would not be fully sampled. Instead, the random sampling would bias against very massive stars, because of their low formation probability, resulting in an actually steeper IMF.

Similarly, an SFH would not be fully sampled when the SFR is low, because a time-averaged continuous (the undersampled) SFR would actually consist of several small “bursts” associated with the formation of new star clusters. Mathematically, the SFH is not fully sampled over a time interval T if $\frac{1}{\langle M_c \rangle} \int_0^T \text{SFR}(t) dt \lesssim 1$, where $\langle M_c \rangle$ is the expected mass of a single star cluster. That is, the SFH is not fully sampled over a specified time interval if the expected number of star clusters formed over that time interval is of order 1 or fewer.¹⁸ da Silva et al. (2012) developed a simulation tool SLUG (Stochastically Lighting Up Galaxies) to study the stochasticity in SF and its effects on SFR indicators and stellar population (da Silva et al. 2014; Krumholz et al. 2015). Using SLUG, Fumagalli et al. (2011) showed that stochasticity is able to explain the observed low $H\alpha$ -to-FUV ratio in local dwarf galaxies (Boselli et al. 2009; Lee et al. 2009; Meurer et al. 2009).

Although evidence of bursty SFHs of dwarf galaxies in the nearby universe has been present through the $H\alpha$ -to-FUV ratio in some of the above studies (e.g., Lee et al. 2009, W12), similar observations have not been conducted beyond the local universe, because of the lack of both deep UV and deep optical/IR spectroscopy data. Low-mass galaxies at higher redshifts are expected to have similar or even burstier SFHs (e.g., Domínguez et al. 2015) compared to their local counterparts. Recently, Kurczynski et al. (2016) found no statistically significant increase of the intrinsic scatter in the SFR- M_* relation at low masses at $0.5 < z < 3.0$, which seems to indicate a gradual assembly of galaxy masses. Their SFRs, however, were measured from SED-fitting of broadband photometry, which traces SFR on timescales of 100 Myr. It, therefore, remains possible that the SF burstiness (indicated by the intrinsic scatter) increases at low masses on timescales shorter than ~ 100 Myr. On the other hand, both non-universal IMF and stochastic SF are phenomena on the scales of star clusters and, therefore, independent of redshift. Studying the redshift evolution of the $H\alpha$ -to-FUV ratio would shed light on the importance of the burstiness of SFHs of low-mass galaxies.

In this paper, to investigate the burstiness of the SFHs beyond the local universe, we use optical spectroscopy from the Team Keck Redshift Survey (TKRS, Wirth et al. 2004) and UV imaging from CANDELS (Grogin et al. 2011; Koekemoer et al. 2011) and the Hubble Deep UV (HDUV) Legacy Survey (HST-GO-13871, PI. Oesch) to measure the ratio of $H\beta$ and

¹⁸ We pause to point out a subtlety in terminology: as used in this statement, a star cluster is simply defined as a collection of stars that formed at a single instant in time, without regard to whether it is gravitationally bound or relaxed, and the implicit assumption we make is that the great majority of stars form in such temporally coherent structures. While most stars do not form in gravitationally bound clusters (e.g., Lada & Lada 2003; Johnson et al. 2016), observations indicate that most stars do form in clusters by the weaker definition of a cluster that is relevant for our purposes (e.g., Lada & Lada 2003; Fall & Chandar 2012). For more discussion on this point, see Krumholz (2014).

FUV (1500 Å) derived SFRs of galaxies at $0.4 < z < 1$ in the CANDELS GOODS-N field. The advantage of using $H\beta$ instead of $H\alpha$ is that the dust extinction effects on $H\beta$ and FUV almost cancel each other out, because they have very similar extinction (assuming the Calzetti law and an extra nebular extinction). Therefore, generally, no extinction correction is needed when measuring the intrinsic ratio of $SFR_{H\beta}$ and $SFR_{1500\text{Å}}$, except for very dusty galaxies (see Sections 3 and 5.5).

We adopt a flat Λ CDM cosmology with $\Omega_m = 0.3$, $\Omega_\Lambda = 0.7$, and the Hubble constant $h \equiv H_0/100 \text{ km s}^{-1} \text{ Mpc}^{-1} = 0.70$. We use the AB magnitude scale (Oke 1974) and a Chabrier (2003) IMF.

2. DATA AND SAMPLE

TKRS observed a magnitude-limited sample of 2911 objects to $R < 24.4$ AB and yielded secure redshifts for 1440 galaxies and active galactic nuclei. TKRS used the 600 lines mm^{-1} grating blazed at 7500 Å. The central wavelength was set at 7200 Å, providing a nominal spectral coverage of 4600–9800 Å at a FWHM resolution of ~ 3.5 Å and $R \sim 2500$. Each slit mask was observed for a total on-source integration time of 3600 s.

We follow Trump et al. (2013) and Guo et al. (2016) to measure the flux of $H\beta$. First, a continuum is fitted across the emission-line region by splining the 50 pixel smoothed continuum. Then, a Gaussian function is fitted to the continuum-subtracted flux in the wavelength region of $H\beta$. The emission-line intensity is computed as the area under the best-fit Gaussian in the line wavelength region. The flux calibration is done by scaling the continuum flux density to match the best-fit stellar population model of the broadband spectral energy distribution (SED) from the CANDELS GOODS-N multiwavelength catalog (Barro et al., in preparation, see Guo et al. (2013) and Galametz et al. (2013) for details). The advantage of this calibration is that using the broadband flux of whole galaxies corrects for the slit-loss effect, under a (reasonable) assumption that the continuum (stellar flux) and emission line have the same spatial distribution. To obtain a reliable flux calibration, we only use galaxies with continuum signal-to-noise ratio $(S/N) > 1 \text{ pixel}^{-1}$. We also require $H\beta$ $S/N > 3$ to use reliable $H\beta$ flux measurements.

The raw $H\beta$ equivalent widths are corrected for stellar absorption according to galaxy ages measured through SED-fitting. As part of the CANDELS SED-fitting effort, each galaxy in our sample has been fitted by 12 SED-fitting codes, which have different combinations of synthetic stellar population models, SFHs, fitting methods, etc. (see Santini et al. (2015) for details). For each galaxy, we use the median of the 12 best-fit ages as its age to measure the stellar absorption from the models of Bruzual & Charlot (2003). The average light-weighted age of galaxies in our sample is almost constant (~ 1 Gyr) from $10^{8.5}$ – $10^{10.5} M_\odot$, corresponding to an average stellar absorption equivalent width of ~ 2.5 Å. We also try to apply a fixed equivalent width of 1 Å (Cowie & Barger 2008; Zahid et al. 2011; Henry et al. 2013) to all galaxies. The smaller stellar absorption equivalent width does not change our results and conclusions, because our galaxies have very large $H\beta$ equivalent widths (a median of ~ 15 Å).

The UV luminosities of galaxies in our sample are measured from *Hubble Space Telescope* (HST)/WFC3 F275W images of

CANDELS UV and HDUV. CANDELS UV covers the CANDELS GOODS-N Deep region in F275W at an approximately four-orbit depth. HDUV intends to add four orbits of observations to each of eight pointings in F275W in the GOODS-N Deep region. We use the first public release (v0.5) of HDUV,¹⁹ which includes five out of the eight new deeper pointings from HDUV, plus all of the CANDELS UV exposures.

The UV photometry is measured in a similar fashion as done for the Ultraviolet Hubble Ultra Deep Field (UVUDF) (Rafelski et al. 2015). SExtractor is run on F275W and ACS/F435W images in dual-image mode with the F435W image as the detection image. An aperture correction is then determined from the F435W band to match the small F435W-band apertures to the larger F160W-band apertures used in the rest of the CANDELS catalog of G. Barro et al. (in preparation). We only include galaxies with F275W $S/N > 5$ in our analyses. There are about 1700 galaxies with F275W $S/N > 5$ at $0.4 < z < 1.0$ in our UV catalog. Our final sample with both $H\beta$ $S/N > 3$ and F275W $S/N > 5$ contains 164 galaxies after excluding X-ray-detected sources.

We use FAST (Kriek et al. 2009) to fit the Bruzual & Charlot (2003) models to the CANDELS GOODS-N multiwavelength catalog to measure M_* . The total SFRs (SFR_{tot}) are measured by combining dust-uncorrected rest-frame UV (2800 Å) and IR luminosities, if the latter (measured from *Spitzer*/MIPS and/or *Herschel*) is available, by following Kennicutt (1998). For these galaxies, $SFR_{\text{tot}} = SFR_{\text{UV+IR}}$. If no IR measurement is available, SFR_{tot} is measured through rest-frame UV (2800 Å) corrected for dust extinction measured from SED-fitting, i.e., $SFR_{\text{tot}} = SFR_{\text{NUV,corr}}$. We refer readers to Barro et al. (2011, 2013) for the details. Because F275W photometry is not used in the SFR_{tot} measurement, SFR_{tot} is independent of our $H\beta$ -to-FUV ratios.

Figure 1 shows that at $M_* > 10^{9.5} M_\odot$, our sample (galaxies with $H\beta$ $S/N > 3$ and continuum $S/N > 1$) is representative of galaxies at $0.4 < z < 1$ in terms of F275W magnitude and total SFR. At $10^{8.5} < M_* < 10^{9.5} M_\odot$, our sample is biased toward UV-bright galaxies (upper panel of Figure 1). This bias is introduced by the TKRS magnitude limit ($R < 24.4$ AB) and our $H\beta$ S/N requirement, the latter of which also biases our sample toward $H\beta$ -bright galaxies. For our goal of measuring the $H\beta$ -to-FUV ratio, we will demonstrate later that the actual effect of our sample selection (combining both $H\beta$ $S/N > 3$ and F275W $S/N > 5$) would bias our results against low $H\beta$ -to-FUV for low-mass galaxies (Section 5.1).

3. MEASURING THE $H\beta$ -TO-FUV RATIO

$SFR_{H\beta}$ and $SFR_{1500\text{Å}}$ are calculated²⁰ through the formula of Kennicutt & Evans (2012)²¹ with an intrinsic $H\alpha/H\beta$ ratio of 2.86 (added as the last term in the right-hand side of Equation (1) below):

$$\log(SFR_{H\beta}) = \log(L_{H\beta}) - 41.27 + \log(2.86), \quad (1)$$

¹⁹ <http://www.astro.yale.edu/hduv/data.html>

²⁰ Throughout the paper, we assume that all the 1500 Å emission is purely stellar, which is a common assumption in most studies. In very young systems with age $\lesssim 1$ Myr, however, nebular emission actually contributes $\sim 20\%$ to the 1500 Å emission (Reines et al. 2010). However, this contribution quickly drops to $\leq 5\%$ as the systems become 5 Myr old. We, therefore, conclude that the nebular contribution to 1500 Å is negligible in our sample.

²¹ Using the recipes of Kennicutt (1998) results in a systematically lower $H\beta$ -to-FUV ratio by 0.03 dex.

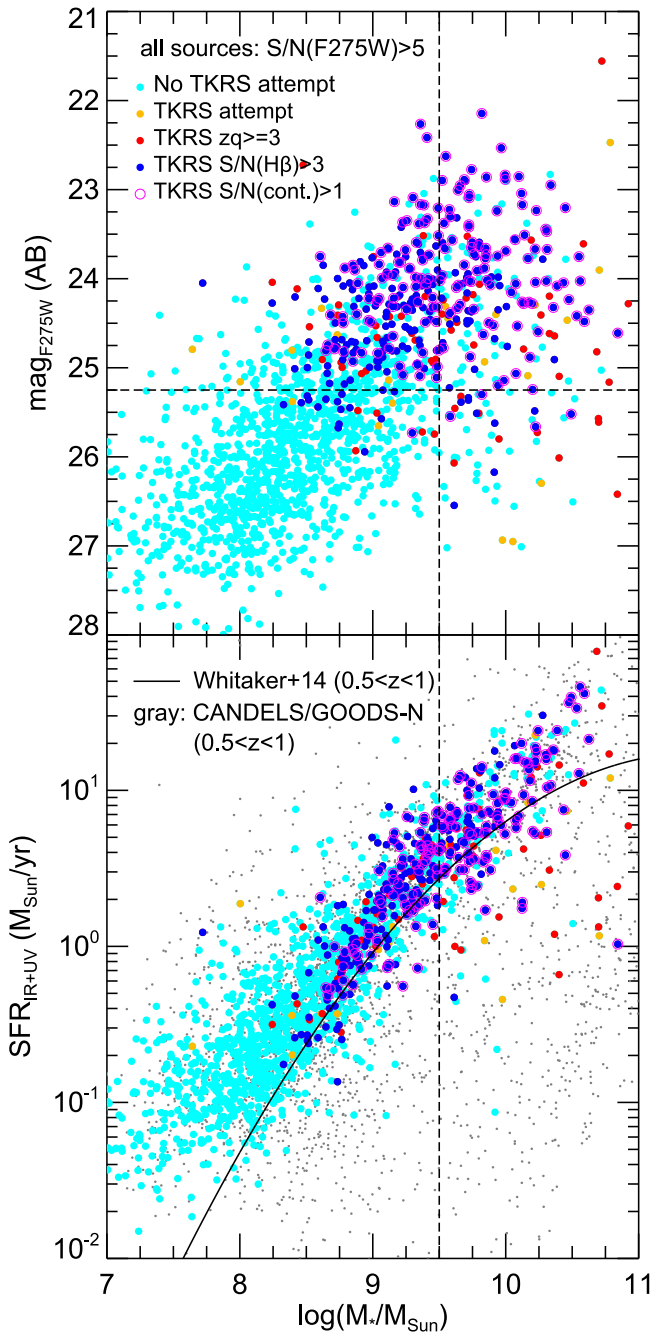


Figure 1. Sample selection. Upper: F275W magnitude– M_* relation for GOODS-N galaxies with F275W S/N > 5. Galaxies with no TKRS attempt are cyan. Those with TKRS attempt, but no secure redshift obtained, are yellow. We only measure $H\beta$ fluxes for galaxies with secure TKRS redshifts (red), and only select those with $H\beta$ S/N > 3 (blue) and continuum S/N > 1 pixel⁻¹ (blue+purple circle) into our sample. Lower: SFR– M_* relation. Galaxies are color coded as labeled in the upper panel. All CANDELS GOODS-N galaxies at $0.5 < z < 1$ are overlotted as gray points. The best-fit relation of Whitaker et al. (2014) is also plotted as a reference (solid line). The method of measuring SFR_{tot} is described in Section 2.

$$\log(\text{SFR}_{1500 \text{ \AA}}) = \log(L_{1500 \text{ \AA}}) - 43.35, \quad (2)$$

where both $L_{H\beta}$ and $L_{1500 \text{ \AA}}$ (νL_ν) are in units of erg s⁻¹. Both formulae have been converted into a Chabrier IMF and assume a solar metallicity.

Low-mass galaxies tend to have subsolar metallicity. The average gas-phase metallicity of $10^{8.5} M_\odot$ galaxies at $z \sim 0.7$ is

about $0.5 Z_\odot$ (Guo et al. 2016). Castellano et al. (2014) showed that using rest-frame UV tends to underestimate the SFRs of subsolar metallicity (gas-phase $\sim 0.3 Z_\odot$) Lyman Break Galaxies at $z \sim 3$ by a factor of a few compared to using SED-fitting or using nebular emission lines. If their results also hold for low-redshift low-mass galaxies, using a UV SFR tracer assuming solar metallicity would artificially increase the $H\beta$ -to-FUV ratio for low-mass galaxies, implying that the intrinsic burstiness of low-mass galaxies is actually stronger than our results.

To calculate the intrinsic SFRs, both $L_{H\beta}$ and $L_{1500 \text{ \AA}}$ should be corrected for dust extinction. A shortcut, however, exists when calculating the ratio of SFR _{$H\beta$} and SFR _{1500 \AA} : extinction correction is negligible, except for very dusty galaxies, because the extinction of $H\beta$ and FUV almost cancel each other out by coincidence. This is an advantage of using $H\beta$ instead of $H\alpha$ in our study.

To illustrate the shortcut, we express the intrinsic $H\beta$ -to-FUV ratio as the following:

$$\begin{aligned} \left(\frac{\text{SFR}_{H\beta}}{\text{SFR}_{1500 \text{ \AA}}} \right)_{\text{int}} &= \left(\frac{\text{SFR}_{H\beta}}{\text{SFR}_{1500 \text{ \AA}}} \right)_{\text{obs}} \times \left(\frac{10^{0.4A(H\beta)}}{10^{0.4A(FUV)}} \right) \\ &= \left(\frac{\text{SFR}_{H\beta}}{\text{SFR}_{1500 \text{ \AA}}} \right)_{\text{obs}} \times 10^{0.4(A(H\beta) - A(FUV))}, \quad (3) \end{aligned}$$

where $A(H\beta)$ and $A(FUV)$ are the attenuation of $H\beta$ and FUV. Their difference is:

$$\begin{aligned} A(H\beta) - A(FUV) &= E(B - V) \times \\ &\left[\frac{k(4861 \text{ \AA})}{0.44} - k(1500 \text{ \AA}) \right], \quad (4) \end{aligned}$$

where the factor of 0.44 is used, because $E(B - V)_{\text{stellar}} = 0.44 \times E(B - V)_{\text{gas}}$ (Calzetti et al. 2000). For the Calzetti attenuation curve (Calzetti et al. 2000),

$$k(4861 \text{ \AA})/0.44 - k(1500 \text{ \AA}) \sim 0.1. \quad (5)$$

Therefore, the factor in Equation (3) to correct for dust extinction is

$$10^{0.4(A(H\beta) - A(FUV))} \sim 10^{0.04E(B - V)_{\text{stellar}}}. \quad (6)$$

For galaxies with $E(B - V)_{\text{stellar}} < 1$, the dust extinction would bias the observed $H\beta$ -to-FUV ratio from the intrinsic one toward the low-value side only by <0.04 dex. Since, on average, the dust extinction of galaxies with $10^{8.5} M_\odot < M_* < 10^{10.0} M_\odot$ is smaller than $E(B - V)_{\text{stellar}} = 0.2$ (Domínguez et al. 2013), this systematic error is negligible compared to other sources of uncertainty.

This shortcut is of course only valid when galaxies have (1) the Calzetti attenuation curve and (2) $E(B - V)_{\text{stellar}} = 0.44 \times E(B - V)_{\text{gas}}$ (or $E(B - V)_{\text{gas}} = 2.27 \times E(B - V)_{\text{stellar}}$). There are other attenuation curves in the literature, e.g., Milky Way (MW)²², Large Magellanic Cloud (LMC), Small Magellanic Cloud (SMC), and recently Mosfire

²² The shortcut is also valid for the MW attenuation curve, but with a slightly higher systematic offset. In this case, the dust extinction would bias the observed $H\beta$ -to-FUV ratio from the intrinsic one toward the low-value side by only <0.07 dex for galaxies with $E(B - V)_{\text{stellar}} < 1$. It is also important to note that the relation $E(B - V)_{\text{gas}} = 2.27 \times E(B - V)_{\text{stellar}}$ in Calzetti et al. (2000) is derived based on the assumption that a Galactic extinction curve applies to the nebular emission.

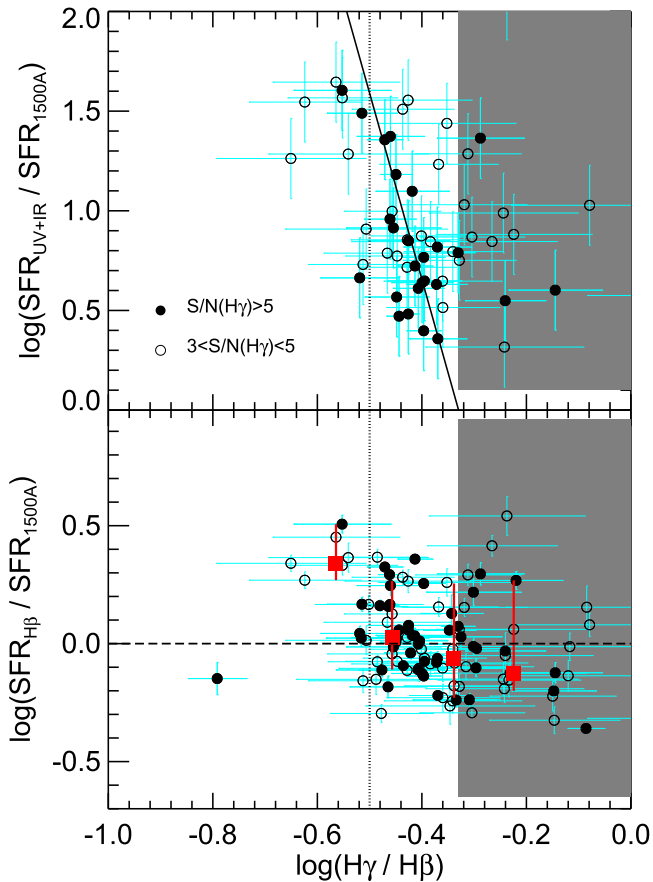


Figure 2. Upper: total-to-FUV SFR ratio as a function of the Balmer decrements ($H\gamma/H\beta$) for galaxies with $S/N(H\gamma) > 3$ (open) and 5 (filled). All galaxies here have IR detections. The solid line shows a fit to galaxies with $S/N(H\gamma) > 5$. The shaded area is where $H\gamma/H\beta > 0.468$, the intrinsic Balmer flux ratio. Lower: $H\beta$ -to-FUV ratio (uncorrected for dust effect) as a function of the Balmer decrements. The median (red squares) and 16th and 84th percentiles (error bars) are measured for both $S/N(H\gamma) > 3$ (open) and > 5 (filled) galaxies. The lower panel has more points than the upper panel, because not every galaxy in the lower panel has an IR measurement.

Deep Evolution Field (MOSDEF) (Reddy et al. 2015, 2016). Moreover, several studies (e.g., Reddy et al. 2010, 2015; Wild et al. 2011; Wuyts et al. 2013) suggest that the extra attenuation of nebular emission, compared to the stellar attenuation, is smaller than what we use here ($E(B - V)_{\text{gas}} = 2.27 \times E(B - V)_{\text{stellar}}$). The extra attenuation depends on the geometry (Wild et al. 2011), SFR (Reddy et al. 2015), and/or specific star formation rate (sSFR; de Barros et al. 2016) of the galaxies. For an attenuation curve other than the Calzetti curve or a smaller-than-2.27 factor for the extra nebular attenuation, the extinction correction factor $10^{0.4(A(H\beta) - A(FUV))}$ in Equation (3) would be significantly smaller than unity, resulting in a non-negligible extinction effect to decrease the observed (dust uncorrected) $H\beta$ -to-FUV ratio (see Section 5.5).

The negligible effect of dust extinction correction in our sample is demonstrated in Figure 2. For a small portion of our sample, we measure the Balmer decrements through the flux ratio of $H\gamma/H\beta$. For galaxies with $H\gamma/H\beta \geq 0.32$ (corresponding to $E(B - V) \leq 0.8$, the vertical dotted line in Figure 2), the dust-uncorrected $H\beta$ -to-FUV ratio has no dependence on $H\gamma/H\beta$ (see Zeimann et al. 2014, for similar results). Only for very dusty galaxies ($H\gamma/H\beta \leq 0.32$, i.e., galaxies with

$\log(H\gamma/H\beta) \lesssim -0.5$ in the lower panel of Figure 2), is the dust-uncorrected $H\beta$ -to-FUV ratio significantly larger than unity, indicating that the dust affects FUV significantly more than it affects $H\beta$. For these galaxies, an extinction correction is needed to measure the $H\beta$ -to-FUV ratio.

The ratio of $SFR_{UV+IR}/SFR_{1500\text{\AA}}$ can serve as a good dust extinction indicator when $H\gamma/H\beta$ measurement is lacking. As shown by the upper panel of Figure 2, the Balmer decrements show a correlation with $SFR_{UV+IR}/SFR_{1500\text{\AA}}$.

We only make a dust correction for galaxies with $SFR_{UV+IR}/SFR_{1500\text{\AA}} > 20$ (corresponding to $H\gamma/H\beta \lesssim 0.32$). We use the best-fit relation in the upper panel of Figure 2 to infer their $H\gamma/H\beta$ ratios and correct for the extinction for $SFR_{H\beta}$. We then use SFR_{UV+IR} as the dust-corrected UV SFR. For these galaxies, the dust-corrected $H\beta$ -to-FUV ratio is, therefore, the ratio of SFR_{UV+IR} and dust-corrected $SFR_{H\beta}$. In our analyses, we use the dust-corrected ratios as the best-measured ratios for these very dusty galaxies, while for other galaxies, whose $SFR_{UV+IR}/SFR_{1500\text{\AA}} < 20$, we use the uncorrected $H\beta$ -to-FUV ratios as their best ratios. Only $\sim 10\%$ of our entire sample are very dusty and, therefore, need the dust-corrected ratios, and they all have $M_* > 10^{9.5} M_\odot$ (purple asterisks in the left panel of Figure 3).

Some galaxies in our sample have $H\gamma/H\beta \geq 0.468$ (the shaded area in Figure 2), which seems to imply that not all galaxies in our sample follow the assumptions of Case B recombination, a requirement of the Kennicutt SFR recipes used in our analyses. We believe that these galaxies are scattered into the shaded area by the large line-ratio uncertainties. Considering the uncertainties (horizontal error bars), 12% of the galaxies with $H\gamma$ measurement in our sample have $H\gamma/H\beta$ larger than 0.468 by more than 1σ , and only 4% are larger than 2σ . This distribution is broadly consistent with a Gaussian distribution with the mean of 0.468, where 16% (and 2%) of the galaxies should be deviated from the mean (0.468) by more than 1σ (and 2σ). We, therefore, argue that the assumption of Case B recombination is not statistically invalid for our sample.

4. RESULTS

Figure 3 shows that the $H\beta$ -to-FUV ratios of the galaxies in our sample increase with their M_* . The median ratio is about 0.7 for galaxies with $M_* \sim 10^{8.5} M_\odot$ and increases to 1.0 for galaxies with $M_* > 10^{9.5} M_\odot$. The trend is broadly consistent with the expectation that the SFHs of lower-mass galaxies are burstier than those of massive galaxies. The figure also shows that the $H\beta$ -to-FUV ratios increase with SFR_{tot} . The median ratio is about 0.7 for galaxies with $SFR < 1 M_\odot \text{ yr}^{-1}$ and increases to ~ 1 for galaxies with $SFR > 10 M_\odot \text{ yr}^{-1}$.

Statistical tests show that the correlation between $H\beta$ -to-FUV ratio and M_* (and SFR) is significant albeit with large scatter. Two coefficients are calculated for our results: (1) Spearman's rank correlation coefficient (r_s), which measures the statistical dependence between two variables and (2) Pearson product-moment correlation coefficient (r), which measures linear correlation between two variables. The correlation between $H\beta$ -to-FUV ratio and M_* (and SFR) is significant: $r_s = 0.39$ (and 0.5), corresponding to a probability of 2.1×10^{-7} (and 4.3×10^{-7}) for the null hypothesis (no correlation) to be accepted. The linear correlation test shows $r = 0.38$ (and 0.47) between $H\beta$ -to-FUV ratio and M_* (and SFR), indicating a modest linear relation. A bootstrapping test

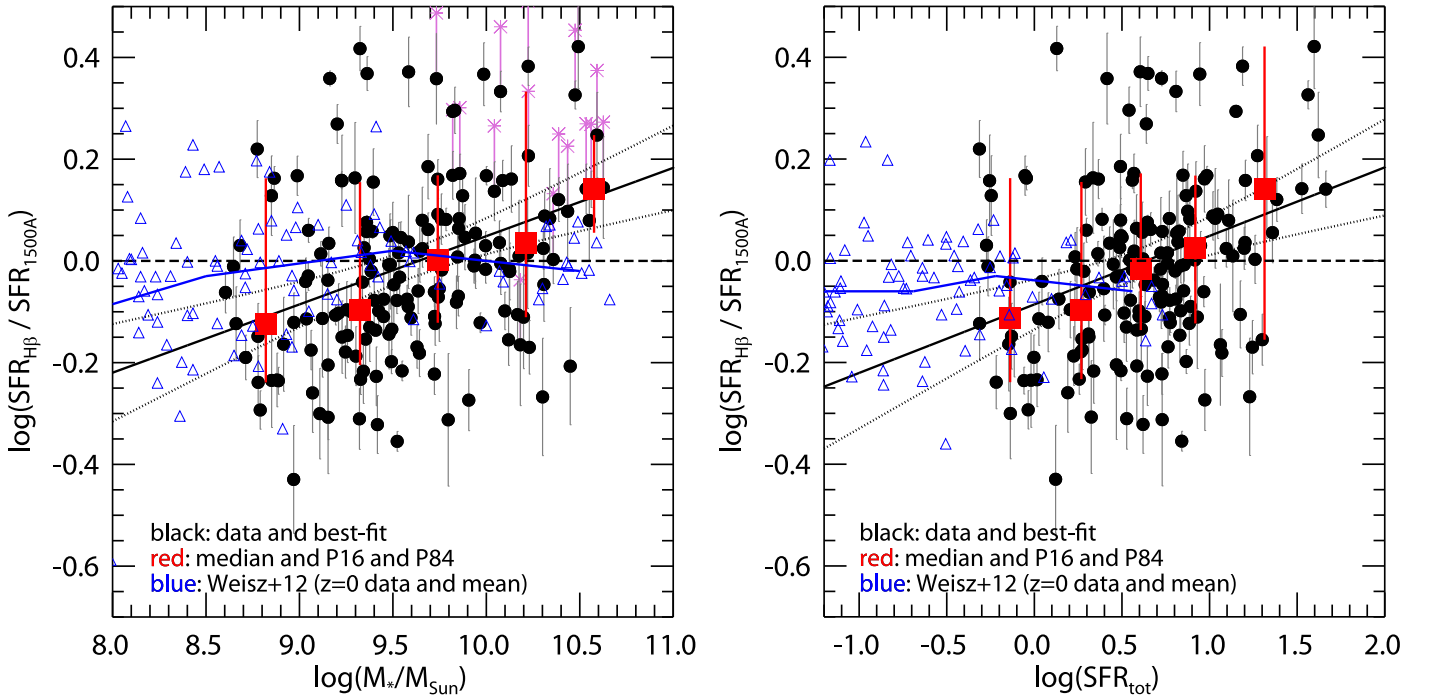


Figure 3. Left: $H\beta$ -to-FUV ratio as a function of M_* . Black circles with gray error bars are the best-measured ratios and their uncertainties. For most of our galaxies, the best-measured ratios are not corrected for dust extinction (see Section 3). However, for very dusty galaxies ($SFR_{UV+IR}/SFR_{FUV} > 20.0$), the best ratios are the ones corrected for dust extinction. As a reference, for such galaxies, their uncorrected ratios are shown as purple stars with purple straight lines connected to their corrected (best) values. Red squares with error bars show the median and 16th and 84th percentiles of each M_* bin. Black solid and dotted lines show the best-fit linear relation and its 95% confidence level. The data of W12 at $z = 0$ are shown as the blue triangles, and their mean is shown by the blue line. Right: similar to the left, but showing $H\beta$ -to-FUV ratio as a function of total SFR (SFR_{tot}). Results of W12 at $z = 0$ are also shown (blue triangles and blue line). Two galaxies with $H\beta$ -to-FUV larger than 0.5 dex are not shown in the figure, but are still included when calculating the median, percentiles, and the best-fit relation.

shows that r of both M_* and SFR has a 5σ significance level. We, therefore, fit a linear relation between $H\beta$ -to-FUV ratio and M_* and SFR in Figure 3.

The large scatter of the results in Figure 3 may be attributed to one or more of the following causes: (1) measurement uncertainties of both $H\beta$ and FUV, (2) galaxy-to-galaxy variation in attenuation/extinction curves (in Section 3, we assume the same extinction curve for all our galaxies), and/or (3) galaxies being observed at different times after the onset of their temporary SF quenched.

We also compare our results with those of W12 at $z = 0$. W12 measured the flux ratio between $H\alpha$ and FUV after correcting for dust extinction. We convert their flux ratios to SFR ratios to obtain a direct comparison with our results. The data of W12 show a ratio near unity from $M_* \sim 10^{10.5} M_\odot$ to $M_* \sim 10^{8.5} M_\odot$. Their ratio starts to become smaller than unity at even lower-mass ranges and eventually reaches 0.7 at $M_* \sim 10^7 M_\odot$, while our ratio already reaches 0.7 at $M_* \sim 10^{8.5} M_\odot$. This difference suggests the existence of redshift evolution of the $H\beta$ -to-FUV ratio for a given M_* .

The correlation between $H\beta$ -to-FUV ratio and SFR in our sample is also different from that of Lee et al. (2009) and W12, after converting their flux ratios to SFR ratios. At $z = 0$, both Lee et al. (2009) and W12 show a constant $H\alpha$ -to-FUV ratio for galaxies with SFRs ranging from $0.1 M_\odot \text{ yr}^{-1}$ – $3 M_\odot \text{ yr}^{-1}$. Their ratio decreases to 0.7 for galaxies with $SFR \sim 0.01 M_\odot \text{ yr}^{-1}$, which is about 50 times smaller than the SFR at which the ratio of our sample reaches the same $H\beta$ -to-FUV ratio. The redshift evolution of the $H\beta$ -to-FUV ratio shown as a function of M_* is also evident as a function of SFR.

Our sample covers a wide range of redshift, because we prefer to include as many galaxies as possible to increase the robustness of the statistics. The cosmic time interval of our sample’s redshift range is about $\Delta t = 3.4$ Gyr, comparable to that from $z \sim 0.4$ to $z \sim 0$ ($\Delta t = 4.3$ Gyr). Therefore, there may also be redshift evolution of the $H\beta$ -to-FUV ratio *within* our sample. To test it, we divided our sample into two redshift bins to calculate the $H\beta$ -to-FUV ratios: $z = 0.4$ – 0.65 ($\Delta t = 1.7$ Gyr) and $z = 0.65$ – 0.95 ($\Delta t = 1.5$ Gyr). We only conduct this test for the M_* range of $10^9 M_\odot$ – $10^{9.5} M_\odot$. Above this mass range, the signal of burstiness is almost zero. Below this mass range, our sample is dominated by galaxies with $z < 0.65$, because of the faintness of low-mass galaxies.

The median $H\beta$ -to-FUV ratios are $\log(H\beta/FUV) = -0.078$ at $z = 0.4$ – 0.65 (38 galaxies with a median redshift of 0.51) and $\log(H\beta/FUV) = -0.110$ at $z = 0.65$ – 0.95 (17 galaxies with a median redshift of 0.79). The cosmic time interval between the medians of the two redshift bins is 1.67 Gyr. The decreasing rate of $\log(H\beta/FUV)$ from the higher-redshift bin to the lower one is, therefore, $(0.110 - 0.078) / 1.67 = 0.019 \text{ dex Gyr}^{-1}$. This rate of redshift evolution *within* our sample is consistent with that between our full $M_* = 10^9 M_\odot$ – $10^{9.5} M_\odot$ sample (with a median $\log(H\beta/FUV) = -0.096$ and a median redshift of 0.53, corresponding to a lookback time of 5.24 Gyr) and $z = 0$ (e.g., W12).

We emphasize that the “redshift evolution” discussed above is for galaxies at the same M_* . We do not trace the mass evolution of the galaxies in our sample, because we are not comparing the progenitors and descendants. Although some individual nearby galaxies’ mass assembly history can be

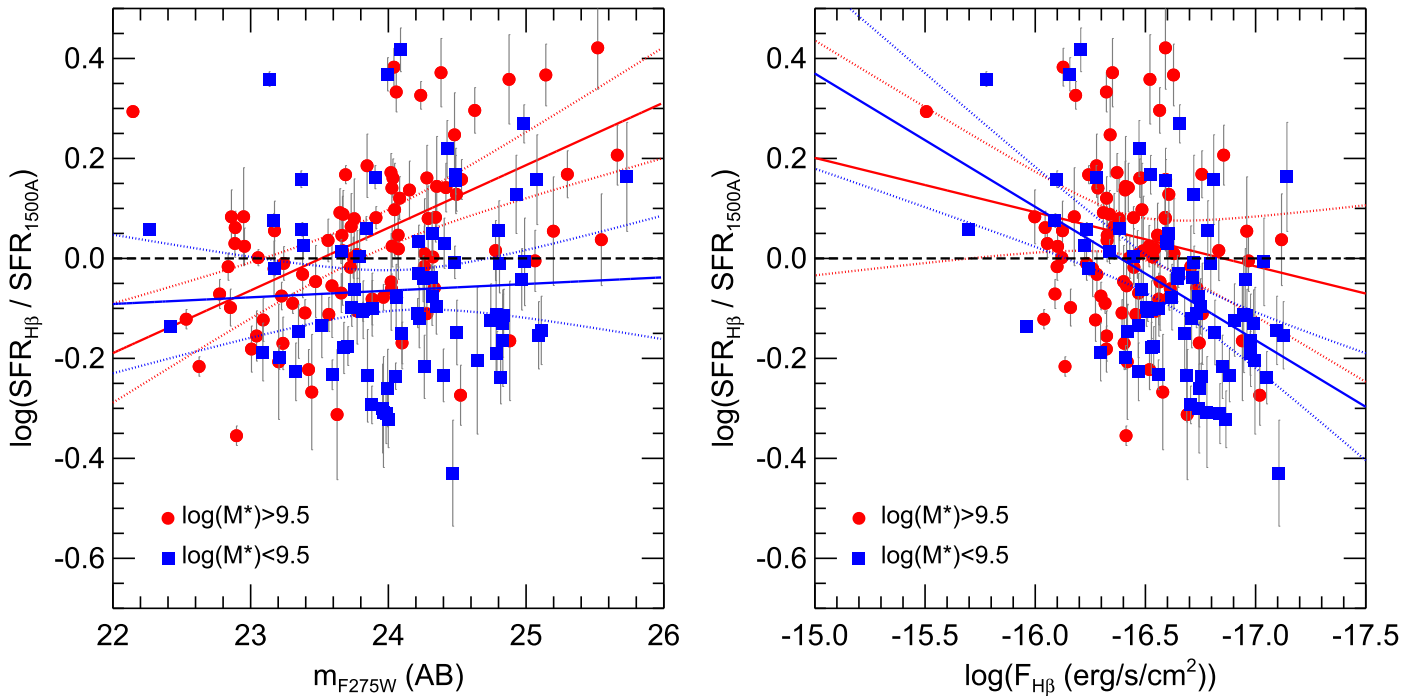


Figure 4. $H\beta$ -to-FUV ratio as a function of the observed F275W magnitude (left) and $H\beta$ flux (right). In each panel, our sample is divided into two M_* bins: $M_* > 10^{9.5} M_\odot$ (red) and $M_* < 10^{9.5} M_\odot$ (blue). A solid line with the same color is the best linear fit to the galaxies in each M_* bin, and the dotted lines with the same color show the 95% confidence level of the fit.

determined (e.g., from Harris & Zaritsky (2009), the LMC increased in $\log(M_*)$ by 0.4 dex between $z \sim 1$ and $z \sim 0$), the knowledge of the average assembly history of low-mass galaxies beyond the local universe is still lacking, which prevents us from comparing the burstiness between progenitors and descendants.

The comparison between galaxies with the same M_* but different redshifts has its own physical motivations, although it cannot trace the evolution of a population. First, the $SFR-M_*$ relation increases with redshift. At the same M_* , higher-redshift galaxies have higher SFR and hence stronger supernova feedback. Second, since the M_* -halo mass relation evolves little with redshifts (Behroozi et al. 2013), the same M_* at different redshifts corresponds to the same halo mass. But at a given halo mass, the cosmic accretion rate increases with redshift (Dekel et al. 2009). Therefore, for the same M_* , higher-redshift galaxies have a higher baryonic accretion rate. As we discussed in Section 1, strong feedback and a high gas accretion rate are necessary to enable the periodic temporary quenching and new accretion bursty cycles. Therefore, at the same M_* , higher-redshift galaxies are expected to be burstier, which is consistent with their observed lower $H\beta$ -to-FUV ratio.

In a recent paper, Zeimann et al. (2014) used the G141 grism of 3D-*HST* (Brammer et al. 2012) to study the $H\beta$ -to-FUV ratio in galaxies at $1.90 < z < 2.35$. Their $H\beta$ SFR is a factor of ~ 1.8 higher than that expected from the systems' rest-frame UV flux density (i.e., $\log(H\beta/FUV) \sim 0.25$). The apparent contradiction between their results and ours can be attributed to two factors: metallicity and age. The sample of Zeimann et al. (2014) is brighter than F140W ~ 25.5 AB and has a median F140W magnitude of ~ 24.5 AB (roughly corresponding to $M_* \sim 10^{9.75} M_\odot$ at their redshifts). We, therefore, only compare their results with our intermediate and massive regimes. First, the sample of Zeimann et al. (2014) has a metallicity distribution ranging from $12 + \log(O/H) \sim 7.2$ to

~ 8.5 with a median of ~ 8.1 . Their median is about 0.6 dex lower than the median metallicity of $10^{9.75} M_\odot$ galaxies at $0.5 < z < 1.0$ (Guo et al. 2016). The formulae used to infer the SFR of local galaxies from $H\beta$ and FUV measurements need to be modified for high-redshift low-metallicity galaxies, as argued by Zeimann et al. (2014). Second, the local formulae assume a system age of 100 Myr. The theoretical $H\beta$ -to-FUV ratio changes little, if any, with age when the age is older than 100 Myr, but the ratio increases quickly as the age decreases when the age is younger than 100 Myr. Therefore, applying the local formulae for the galaxies in our sample (with a median age of 1 Gyr) is reasonable, but the formula need to be modified for the high-redshift strong- $H\beta$ galaxies of Zeimann et al. (2014), which are likely younger than 100 Myr.

5. DISCUSSION

There are four possibilities to explain the low $H\beta$ -to-FUV ratio of low-mass and/or low-SFR galaxies: (1) sample selection, (2) non-universal IMF, (3) stochastic SF on star or star cluster scales, and (4) bursty SFH on galactic scales. We will show that (1), (2), and (3) are not able to plausibly explain the observed ratios alone, and, therefore, (4) is also needed. We also add a detailed discussion on the effect of dust extinction correction in this section.

5.1. Sample Selection Effect

One of our main sample selection criteria is $H\beta$ S/N > 3 , which biases our sample against $H\beta$ -faint galaxies and, therefore, would artificially increase the $H\beta$ -to-FUV ratio. A second bias, however, is introduced by our UV cut of F275W S/N > 3 (Figure 1), which biases our sample against UV-faint galaxies and would artificially decrease the $H\beta$ -to-FUV ratio. Which of the two biases dominates determines the actual systematic bias in our observed $H\beta$ -to-FUV ratio.

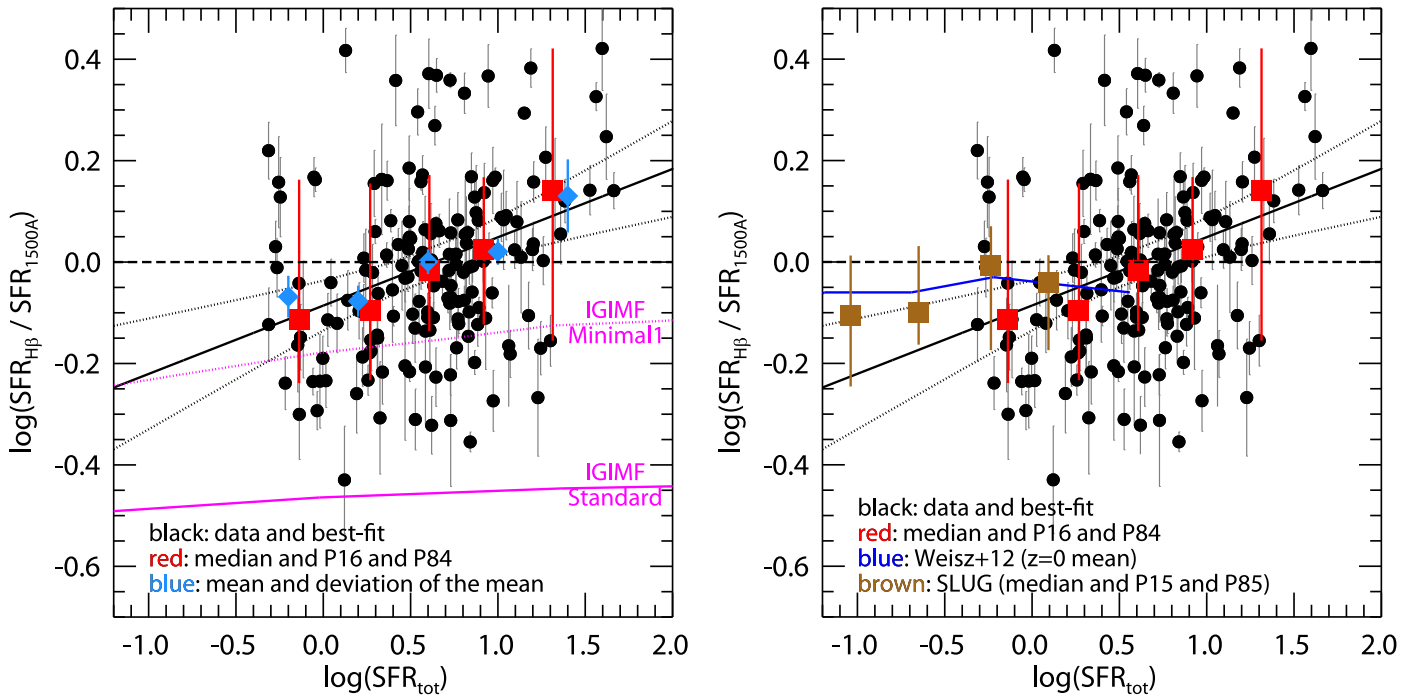


Figure 5. Comparisons between our observed $\text{H}\beta$ -to-FUV ratio (as a function of total SFR) and the predictions of two IGIMF models (left) and the SLUG simulations (right). In both panels, black circles with gray error bars are the best-measured ratios and their uncertainties from our observations. Red squares with error bars show the median and 16th and 84th percentiles of the black circles in each SFR bin. Blue symbols with error bars in the left panel show the mean and the standard deviation of the mean of each SFR bin. Black solid and dotted lines show the best-fit linear relation and its 95% confidence level of the black circles. The predicted $\text{H}\beta$ -to-FUV ratios of the two IGIMF models are shown by the purple lines in the left panel. The predicted $\text{H}\beta$ -to-FUV ratios of the SLUG simulations are shown by the brown squares with error bars in the right panel.

Figure 4 plots the $\text{H}\beta$ -to-FUV ratio as a function of both F275W magnitude and $\text{H}\beta$ flux. For galaxies with $M_* < 10^{9.5} M_\odot$, their median $\text{H}\beta$ -to-FUV ratio is almost independent of their F275W magnitudes (blue in the left panel), but decreases with their $\text{H}\beta$ fluxes (blue in the right). This result suggests that the $\text{H}\beta$ flux limit is the main factor that biases our results: if we had a deeper spectroscopic sample to extend the trends in the right panel of Figure 4 to lower $\text{H}\beta$ flux, we would obtain an even lower median $\text{H}\beta$ -to-FUV ratio for the low-mass galaxies. On the other hand, including fainter UV galaxies from deeper F275W images would not affect our results, because the median $\text{H}\beta$ -to-FUV ratio is almost independent of the F275W magnitudes. Therefore, our current sample selection biases our $\text{H}\beta$ -to-FUV ratio of low-mass galaxies against the low-value side, implying that a complete sample of low-mass galaxies might have even lower intrinsic $\text{H}\beta$ -to-FUV ratios than what we find.

5.2. Non-universal IMF

Typically, an IGIMF model assumes that (1) all stars form in clusters (e.g., Pflamm-Altenburg et al. 2007); (2) the cluster mass function is a power law; (3) the mass of the most massive star cluster (i.e., the truncation mass of the power law) is a function of the total SFR of a galaxy; and (4) the mass of the most massive star in a star cluster is a function of the mass of the cluster. These assumptions result in a low $\text{H}\alpha$ -to-FUV ratio by reducing the probability of forming massive stars in low-SFR galaxies. Pflamm-Altenburg et al. (2007, 2009) presented the predicted $\text{H}\alpha$ -to-FUV ratio as a function of $\text{SFR}_{\text{H}\alpha}$ for a few IGIMF models. Here, we compare two of their models to our observations: *Standard* and *Minimal1* (see Table 1 of Pflamm-Altenburg et al. 2007). The Standard and Minimal1

models differ in the assumed cluster mass functions. The Minimal1 scenario uses a cluster mass function that follows $dN/dM \propto M^{-2}$ over most of its mass range in accord with most observational determinations of the cluster mass function (e.g., see the review by Krumholz (2014)). In contrast, the Standard model assumes a steeper $dN/dM \propto M^{-2.35}$ slope, i.e., it assumes that the cluster mass function has the same slope as the stellar IMF. The latter choice generates a much stronger IGIMF effect, because it places more of the SF in smaller clusters with more strongly truncated IMFs. We convert their predicted $\text{H}\alpha$ -to-FUV ratios from a function of $\text{SFR}_{\text{H}\alpha}$ to a function of SFR_{FUV} (equivalent to SFR_{tot} as their models are dust free) and compare them with our $\text{H}\beta$ -to-FUV ratio as a function of SFR_{tot} .

Figure 5 shows that the Standard IGIMF model significantly underpredicts the ratio by a factor of three for all galaxies, because of its severely reduced probability of forming massive stars. Moreover, the slopes of both Standard and Minimal1 models are flatter than our observed results. The difference of the slopes would be even larger, if our sample selection effect, which preferentially excludes galaxies with low $\text{H}\beta$ -to-FUV (Section 5.1), is taken into account. The Minimal1 model lies within the 1σ level of the *scatter* of our sample. Its prediction is close to our observed ratios for galaxies with $\text{SFR} \sim 1 M_\odot \text{ yr}^{-1}$, but it underpredicts the ratio for higher-SFR galaxies. To statistically test the acceptance (or rejection) of the Minimal1 model, we calculate the goodness-of-fit (reduced χ^2) of the Minimal1 model to the mean and the standard deviation of the mean of our results (blue points and error bars in Figure 5). The reduced χ^2 is ~ 22 , much larger than unity, and hence rules out the Minimal 1 model with more than 5σ confidence.

We, therefore, conclude that the two types of IGIMF models are unable to provide a plausible explanation of our results.

Similar results have been reported by W12. They found that the Minimal1 model matches their results at $z = 0$ well for galaxies with $M_* > 10^8 M_\odot$ and/or $\text{SFR}_{\text{H}\alpha} > 0.01 M_\odot \text{yr}^{-1}$, while the Standard model systematically underpredicts the $\text{H}\alpha$ -to-FUV ratio.

5.3. Stochastic SF on Small Scales

The stochasticity considered here consists of stochastic sampling of both the IMFs and SFHs (see Section 1). As shown by Lee et al. (2009) and Fumagalli et al. (2011), stochastic sampling of IMFs alone cannot reproduce the entire range of the observed $\text{H}\alpha$ -to-FUV ratio, because it predicts a systematically high value for very low-SFR local galaxies.

To fully describe the stochasticity, the simulation code SLUG (da Silva et al. 2012, 2014; Krumholz et al. 2015) synthesizes stellar populations using a Monte Carlo technique to properly treat stochastic sampling including the effects of clustering, IMF, SFH, stellar evolution, and cluster disruption. Using SLUG, Fumagalli et al. (2011) showed that stochasticity is able to explain the observed low $\text{H}\alpha$ -to-FUV ratio in local dwarf galaxies. Here, we compare the SLUG simulations with our results to test if stochastic SF can explain our observed $\text{H}\beta$ -to-FUV ratio at $0.4 < z < 1.0$. Among all SLUG models, we use the one that has the most significant stochastic effects by assuming all stars are formed in clusters. Also, the SLUG simulations are run to $z = 0$.

Figure 5 shows that the SLUG's prediction of $\text{H}\beta$ -to-FUV ratio (brown squares with error bars) is systematically higher than the median of our observed values. SLUG provides predictions only for galaxies with $\log(\text{SFR}) < 0.5$, while our sample contains only galaxies with $\log(\text{SFR}) > -0.5$. The range of SFRs covered by both the predictions and observations is narrow. Nevertheless, the comparison suggests that the stochastic SF alone is not able to explain the low $\text{H}\beta$ -to-FUV ratio of low-SFR galaxies in our sample.

SLUG's predictions match the results of local dwarf galaxies of W12 very well. The good agreement between SLUG and local observations (see also Fumagalli et al. (2011) for comparison with observations before W12) and the systematic offset of SLUG from our results suggest that, compared to the local universe, an extra source is needed to fully explain the observed $\text{H}\beta$ -to-FUV ratio at $z \sim 0.7$.

5.4. Burstiness of Low-mass Galaxies

Because neither non-universal IMF nor stochastic SF is able to fully explain our data, we believe that a bursty SFH is needed for low-mass galaxies at $z \sim 0.7$. This speculation is supported by the systematically lower $\text{H}\beta$ -to-FUV ratio at $z \sim 0.7$ compared to that at $z = 0$. The main driver of the bursty SFH is gas expulsion due to feedback followed by new gas accretion (or recycling). This driver would be more efficient at high redshift when the cosmic gas accretion rate is high and when galaxy dynamic timescales are short. Therefore, if low-mass galaxies are bursty, the $\text{H}\beta$ -to-FUV ratio at high redshift is expected to be lower than that at low redshift, which is consistent with our data.

One additional piece of evidence of the bursty SFH is the relation between the $\text{H}\beta$ -to-FUV ratio and the sSFR in Figure 6. The $\text{H}\beta$ -to-FUV ratio clearly increases with sSFR when sSFR

is measured through a nebular emission line, while the ratio is almost constant over a wide sSFR range when sSFR is measured through UV+IR or dust-corrected UV. The trend with $\text{H}\beta$ sSFR is consistent with galaxies undergoing starbursts: at the onset of a starburst, nebular emission-line luminosity increases faster than FUV luminosity, resulting in a high $\text{H}\beta$ sSFR and a high $\text{H}\beta$ -to-FUV ratio; while at the end of the burst (or at the onset of temporary quenching), emission-line luminosity decreases faster than UV luminosity, resulting in low $\text{H}\beta$ sSFR and a low $\text{H}\beta$ -to-FUV ratio. The duration of a burst is likely much less than ~ 100 Myr, because when the UV+IR or dust-corrected UV sSFR (an indicator averaged over 100 Myr) is used, the trend disappears and the $\text{H}\beta$ -to-FUV ratio remains a constant over a wide range of sSFR. Kurczynski et al. (2016) also found no statistically significant increase of the intrinsic scatter in the $\text{SFR}-M_*$ relation at low masses at $0.5 < z < 3.0$ when the SFRs are measured from SED-fitting of broadband photometry, which traces SFR on timescales of 100 Myr. Their results also indicate that if the bursts exist, their timescale is likely much less than ~ 100 Myr.

The importance of burstiness for low-mass galaxies can be investigated through SFH models. W12 constructed a series of models of bursty SFHs to explain the observed $\text{H}\alpha$ -to-FUV ratio at $z = 0$. We use their models to explain our results.

Their models assume an underlying constant SFH with normalized $\text{SFR} = 1$ and superposed with several starbursts over a period of 500 Myr. The bursts are characterized by three key parameters: the burst amplitude (A , the increasing factor of SFR over the underlying constant SFR during the burst duration), burst duration (D), and burst period (P). The value of $(D \times A)/P$ indicates the relative importance of the bursty SF phase on SFR compared to the constant SF phase.

As discussed in W12, it is the distribution of $\text{H}\alpha$ -to-FUV ratios contains information about the burstiness of the galaxies. We, therefore, calculate the burstiness of our sample by matching the $\text{H}\alpha$ (or $\text{H}\beta$)-to-FUV ratio distributions. We divide all galaxies in our sample into five M_* bins, starting from $10^{8.5} M_\odot$ and each spanning 0.5 dex. For each bin (called our bin), we try to find a M_* bin in the W12 sample, where the W12 galaxies have the most similar $\text{H}\alpha$ -to-FUV distribution with the $\text{H}\beta$ -to-FUV distribution of the galaxies in our bin. Specifically, for each of our bins, we run the K-S test to compare its $\text{H}\beta$ -to-FUV distribution with the $\text{H}\alpha$ -to-FUV distributions of a series of mass bins of W12. This series of mass bins consist of many bins with width of 1 dex. The smallest bin starts from $10^6 M_\odot$, and each of the next bin increases its lower-mass limit by 0.2 dex. These bins are designed to be non-exclusive and their widths are wider than that of our bin to provide robust statistics. The W12 bin that has the largest K-S test probability has the most similar $\text{H}\alpha$ (or $\text{H}\beta$)-to-FUV to our bin. For example, the M_* bin of $\log(M_*/M_\odot) = [9.0, 9.5]$ in our sample has the largest K-S probability (0.94) with the M_* bin of $\log(M_*/M_\odot) = [7.5, 8.5]$ in W12. We then use the burstiness of the bin of $[7.5, 8.5]$ in W12 (interpolate from Table 4 of W12) as the burstiness of our $[9.0, 9.5]$ bin. We repeat this calculation for all our bins and the results are shown in Figure 7. The error bars are measured from a bootstrapping test, which only samples three quarters of the galaxies in each of our bins and repeats the random sampling 100 times.

Figure 7 shows that the median of $(D \times A)/P$ in our sample increases toward lower M_* . The three parameters in

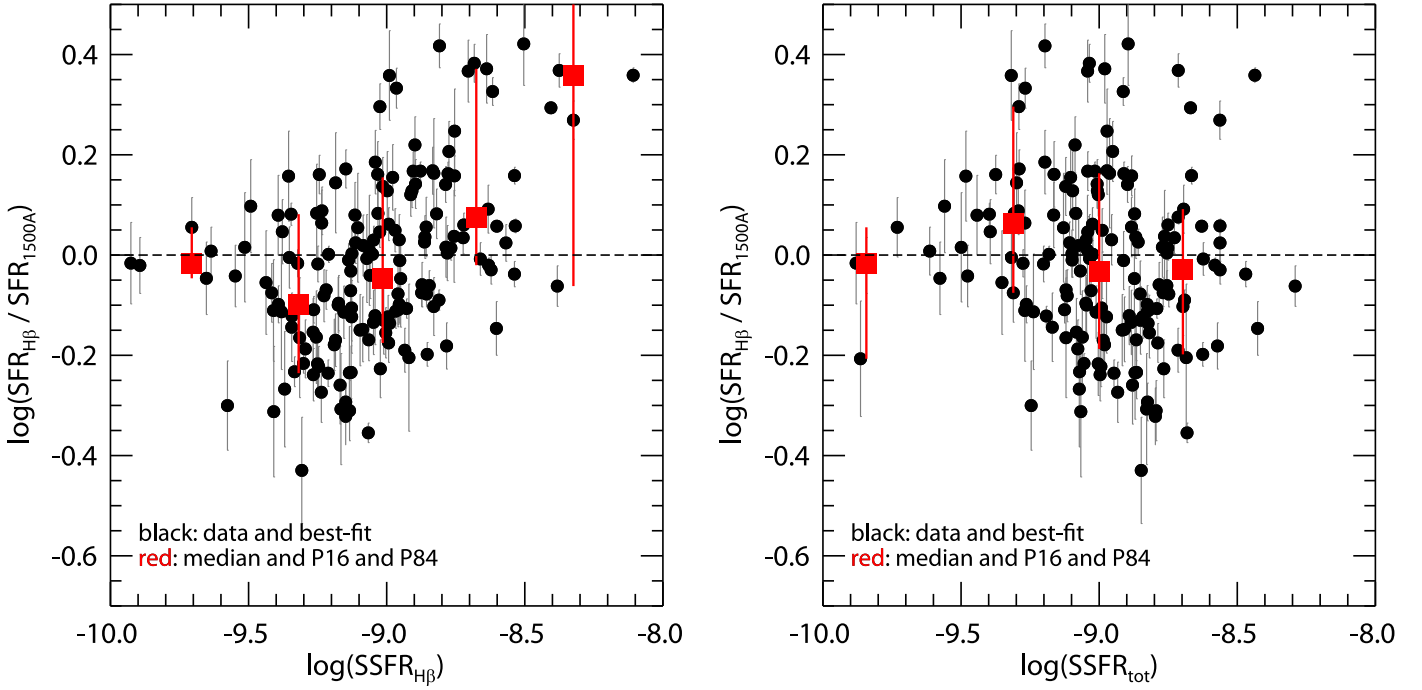


Figure 6. $H\beta$ -to-FUV ratio as a function of sSFR. Left: sSFR is calculated by using dust-corrected $H\beta$ -derived SFR, where the dust extinction is measured through the ratio of SFR_{tot}/SFR_{FUV} (see the upper panel of Figure 2). Right: sSFR is calculated by using SFR_{tot} . In both panels, black circles with gray error bars are the best-measured ratios and their uncertainties from our observations. Red squares with error bars show the median and 16th and 84th percentiles of the black circles in each sSFR bin.

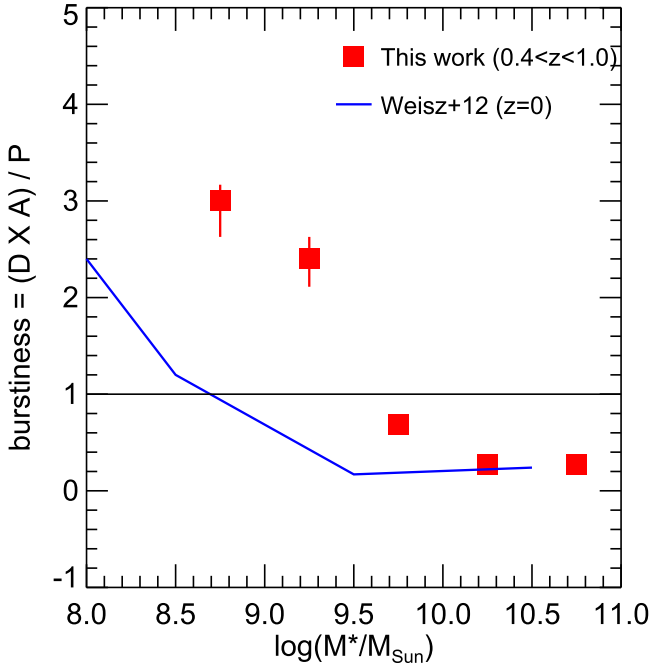


Figure 7. Burstiness of the SFHs of our galaxies. The burstiness, $(D \times A)/P$, is measured from SFH models of W12 (see Section 5.4 for details). Red squares and error bars show the burstiness and 1σ confidence level of our sample. The result of W12 at $z = 0$ is shown as the blue line.

$(D \times A)/P$, however, are coupled. A high $(D \times A)/P$ can be caused by either true starbursts (i.e., $P \gg D$ and $(D \times A) \gg P$) or “gasping” SFHs (i.e., a short decrease in the SFR from an otherwise constant rate with $A \gg 1$ and $P \lesssim D$). The best W12 models used in our figures all have

$P \gg D$ with an average $P \sim 250$ Myr and D of a few tens of megayears, indicating a true “burst” model.

The most massive galaxies have the median $(D \times A)/P \sim 0$, suggesting their SFH is basically constant over timescales of 500 Myr. Intermediate-mass galaxies have median $(D \times A)/P \sim 1$, suggesting an almost equal contribution of SFRs from both bursty and constant SF phases. For low-mass galaxies, the median $(D \times A)/P > 1$, suggesting that most of the SF occurs during the bursty phase. At $M_* \sim 10^{8.5} M_\odot$, the bursty phase contributes a factor of three more SF than the constant phase does.

We also compare our results with those of W12 at $z = 0$. Our burstiness $(D \times A)/P$ is larger than theirs at a given M_* . In their sample, the bursty phase becomes comparable to the constant phase only with galaxies at $M_* < 10^{8.5} M_\odot$. But in our sample, it occurs at $M_* \sim 10^{9.5} M_\odot$. The difference again clearly shows the redshift evolution of the burstiness: at a given M_* , galaxies at higher redshift are burstier, i.e., have more of their SF occurs during the bursty phases.

Our results of low-mass galaxies being burstier than massive galaxies also show excellent agreement with that from the Feedback in Realistic Environments (FIRE) simulations (Hopkins et al. 2014). Sparre et al. (2015) measured both $H\alpha$ and FUV SFRs of the FIRE galaxies and found that the $H\alpha$ -to-FUV ratio in FIRE decreases toward small M_* . The FIRE ratio is unity at $10^{10} M_\odot$ and decreases to ~ 0.7 at $10^{8.5} M_\odot$, matching our observed results surprisingly well. The FIRE galaxies exhibit order-of-magnitude SFR variations over timescales of ~ 10 Myr. Consequently, low-mass galaxies can go through both quenched (in terms of the 10 Myr averaged SFR) and starburst phases a few times within a 200 Myr period. The FIRE galaxies, however, are at redshifts lower than ours: $z = 0.0, 0.2$, and 0.4 . The FIRE $H\alpha$ -to-FUV ratio is also systematically smaller than that of W12, indicating that the

FIRE galaxies are slightly burstier than the observed local galaxies.

Our results are also consistent with other indicators of bursty SFH. A model of Forbes et al. (2014) suggests that the scatter in both M_* -SFR and M_* -gas-phase metallicity relations is mainly governed by the dispersion of the baryonic accretion rate and/or the dispersion of the M_* -halo mass relation. Therefore, the increase of scatter toward the low-mass regime in one relation would be accompanied by an increase in the other. Our observed $H\beta$ -to-FUV trend implies that the scatter in the M_* -SFR relation would increase with the decreasing of M_* . Therefore, the scatter in the M_* -gas-phase metallicity relation should also increase toward the low-mass regime. Indeed, Guo et al. (2016) found such an increase of the scatter in the M_* -gas-phase metallicity relation toward low-mass regimes, which reinforces the bursty SFHs of low-mass galaxies at $z \sim 0.7$.

5.5. Effects of Dust Extinction Correction

Our “shortcut” of ignoring dust correction is enabled by the choice of the Calzetti attenuation curve. The Calzetti curve was derived through local starburst galaxies. Because the normalization of the SFR- M_* relation increases with redshift, local starburst galaxies would be the analogs of higher-redshift normal star-forming galaxies, which makes the Calzetti curve possibly an appropriate and the most commonly used one in the studies of distant (e.g., $z > 0.5$) galaxies. Choosing the Calzetti curve would make our paper consistent with other studies of distant galaxies. For example, M_* of the galaxies in our sample is measured through SED-fitting with the Calzetti curve (Santini et al. 2015). The dependence of our results on the choice of the attenuation curve, however, needs to be discussed.

For this purpose, we measure the FUV-NUV color of each galaxy and then derive its slope (β) of the rest-frame UV continuum. The UV slope provides a measurement of the stellar extinction $E(B - V)_{\text{stellar}}$. We then derive the gas extinction through $E(B - V)_{\text{stellar}} = 0.44 \times E(B - V)_{\text{gas}}$. With the extinction of both gas and stellar components in hand, we then derive the extinction correction factor $A(H\beta) - A(\text{FUV})$, i.e., Equation (5), by using four different attenuation curves: (1) Calzetti (Calzetti et al. 2000); (2) Milky Way (Cardelli et al. 1989); (3) SMC Bar (Gordon et al. 2003); and (4) LMC average (Gordon et al. 2003). The results (median and 16th and 84th percentiles) of the *dust-corrected* $H\beta$ -to-FUV ratios of our sample are shown as blue stars and error bars in Figure 8. The red squares and error bars show our original results of using the “shortcut” to ignore dust correction.

The new results with dust extinction corrected by using the Calzetti, Milky Way, and LMC average attenuation curves are not significantly different from our original results of ignoring dust. The tiny difference between the dust corrected (black circles) and uncorrected (gray stars), especially for low-mass galaxies, validates our “shortcut” of ignoring the dust correction. Therefore, our analyses and conclusions of the burstiness of low-mass galaxies would not be significantly changed if these three curves are used.

The only different result comes from the SMC curve, which changes the $H\beta$ -to-FUV ratio of massive galaxies more than that of low-mass galaxies due to the higher dust extinction of massive galaxies. In this case, the $H\beta$ -to-FUV ratio is almost constant around -0.2 for all masses and seems to match the

prediction of the IGIMF Minimal1 model (the purple dotted line in the left panel of Figure 5). However, as shown by other studies, the SFRs measured from FUV and nebular emission line are usually in very good agreement for massive galaxies (see W12 for $z = 0$ galaxies and Shivaie et al. (2015, 2016) for $z \sim 2$ galaxies). Therefore, we suspect that the SMC curve “over-corrects” the dust extinction for massive galaxies to push their $H\beta$ -to-FUV ratios to being significantly smaller than unity (i.e., negative in logarithmic scale).

So far, we still have one assumption untested, namely $E(B - V)_{\text{stellar}} = 0.44 \times E(B - V)_{\text{gas}}$. The factor of 0.44 (called star-to-gas factor) is argued to be a lower limit and the actual value may vary according to the properties of the galaxies as well as the chosen attenuation curves. Here, we test its relation with the attenuation curves. For this purpose, we assume that any valid combination of the attenuation curve and the star-to-gas factor would cause massive ($> 10^{10} M_{\odot}$) galaxies to have the $H\beta$ -to-FUV ratio equal to unity. By minimizing the residual of the $H\beta$ -to-FUV ratio of massive galaxies to unity, we find that the best star-to-gas factor is 0.50 for the Calzetti curve, 0.51 for MW, 0.33 for SMC, and 0.48 for LMC. Applying these values to each attenuation curve would not significantly change our original results (i.e., low-mass galaxies have $\log(H\beta/\text{FUV}) \sim -0.2$). Our main conclusions of the burstiness of low-mass galaxies are thus still valid.

In conclusion, we test different extinction curves and different reasonable star-to-gas factors. Our main conclusions hold for almost all of our choices, except for the SMC curve with the star-to-gas factor of 0.44. It is important to note that we always assume all galaxies have the same attenuation curve and star-to-gas factor. There may be galaxy-to-galaxy variation. On the other hand, however, none of our choices would increase the $H\beta$ -to-FUV ratio of low-mass galaxies to be significantly larger than unity (positive in logarithmic scale). Therefore, even if the galaxy-to-galaxy variation exists, our results of a smaller-than-unity median $H\beta$ -to-FUV ratio for low-mass galaxies are still robust.

Finally, another possible explanation of the observed $H\beta$ -to-FUV ratio has not been discussed in our paper: the loss of ionizing photons. Our emission-line SFR calibration assumes that every emitted Lyman continuum photon results in the ionization of a hydrogen atom. This assumption may be invalid due to either of the two effects: (1) leakage of Lyman continuum photons into the intergalactic medium and (2) absorption of Lyman continuum photons by dust internal to the HII region. The loss of ionizing photons would result in a lower-than-unity $H\beta$ -to-FUV ratio. The two effects, however, may be negligible for our low-mass galaxies. The Lyman continuum escape fraction is less than 2% for galaxies at $z \sim 1$ (Siana et al. 2007, 2010; Rutkowski et al. 2016). And the dust absorption would preferentially affect massive (and hence dustier) galaxies rather than low-mass systems.

6. CONCLUSIONS

We study the ratio of SFRs measured from $H\beta$ and FUV for galaxies at $0.4 < z < 1$ in the CANDELS GOODS-N region by using the TKRS Keck/DEIMOS spectroscopy and the newly available *HST*/WFC3 F275W images from CANDELS and HDUV. Our goal is to investigate the burstiness of the SFHs of low-mass galaxies by using the $H\beta$ -to-FUV ratio ($\text{SFR}_{H\beta}/\text{SFR}_{1500 \text{ \AA}}$). Our sample contains 164 galaxies down to $M_* = 10^{8.5} M_{\odot}$. An advantage of using $H\beta$ instead of $H\alpha$ is

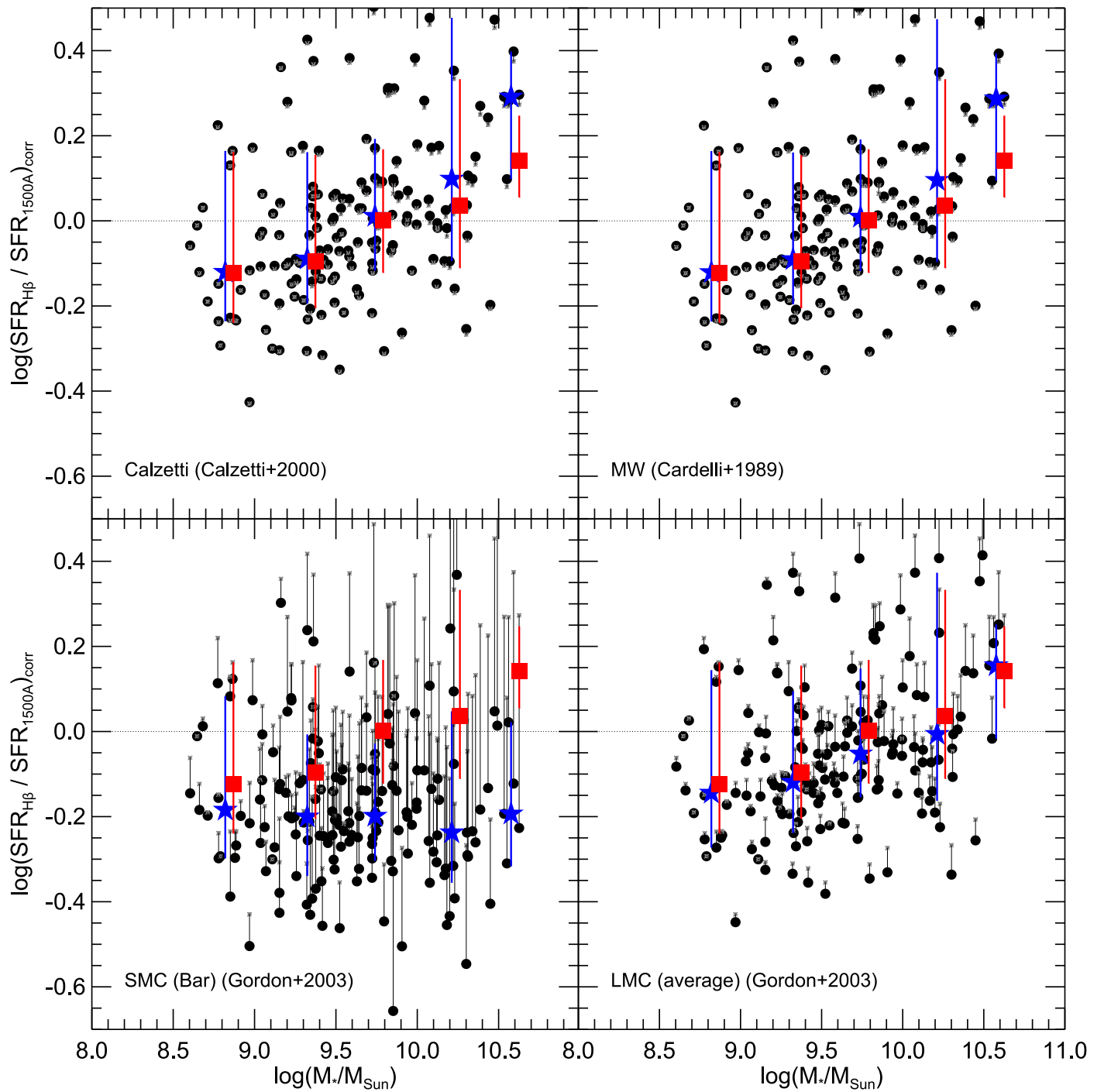


Figure 8. Test of the $H\beta$ -to-FUV ratios on the choice of the dust attenuation curve. Each panel shows the *dust-corrected* $H\beta$ -to-FUV ratio as a function of M_* , by using a certain dust attenuation curve as indicated in the lower-left corner of each panel. Black circles show the *dust-corrected* values, while gray stars connected to the black circles show the *uncorrected* values. Blue stars with error bars show the median and 16th and 84th percentiles of the *dust-corrected* ratios (i.e., black circles) of each M_* bin. Red squares with error bars show the median and 16th and 84th percentiles of the original ratios of each M_* bin by using the shortcut of ignoring dust correction, which are the same as those in the left panel of Figure 3.

that the dust extinction effects on $H\beta$ nebular line and on FUV stellar continuum (1500 \AA) almost cancel each other out, so that the dust extinction correction is negligible for most of our galaxies when the ratio of $H\beta$ and FUV is measured.

We find that the $H\beta$ -to-FUV SFR ratio increases with M_* and SFR. The median $\text{SFR}_{H\beta}/\text{SFR}_{1500 \text{ \AA}}$ ratio at $M_* \sim 10^{8.5} M_\odot$ is lower than that at $M_* \sim 10^{10} M_\odot$ by a factor of 0.7. In terms of total SFR, the median $H\beta$ -to-FUV ratio of galaxies with $\text{SFR} \sim 0.5 M_\odot \text{ yr}^{-1}$ is about 0.7 times lower than

that with $\text{SFR} \sim 10 M_\odot \text{ yr}^{-1}$. We also find that at $M_* < 10^{9.5} M_\odot$, our median $H\beta$ -to-FUV is lower than that of local galaxies at the same M_* , implying a redshift evolution. Our sample selection biases our results against low $H\beta$ -to-FUV ratios, suggesting that the true $H\beta$ -to-FUV ratio is even lower for a complete sample of low-mass galaxies, which strengthens our results.

One model of non-universal IMF (IGIMF) scenario broadly matches our results for galaxies with $\text{SFR} \sim 1 M_\odot \text{ yr}^{-1}$, but

cannot match the increase of the $H\beta$ -to-FUV ratio toward higher-SFR galaxies. Compared to our results, SLUG simulations of stochastic SF on star cluster scales overpredicts the $H\beta$ -to-FUV ratio for low-SFR galaxies.

Bursty SFHs provide a plausible explanation for the observed $H\beta$ -to-FUV ratios of low-mass galaxies at $z \sim 0.7$. The burstiness increases as M_* decreases. For galaxies with $M_* < 10^9 M_\odot$, the SF burstiness is as large as three, namely, within a period of ~ 500 Myr, the amount of SF occurring in starburst phases is three times larger than that in a smooth continuous phase. The burstiness of galaxies with $M_* > 10^{10} M_\odot$ is < 1 , namely, more stars formed in the smooth continuous phase than in bursty phases.

The bursty SF plays an important role in the assembly of low-mass galaxies. Future work can improve our knowledge of it from three aspects: (1) deeper UV imaging (e.g., UV Frontier Fields) and deeper spectroscopy (e.g., Halo7D) to explore even lower M_* regimes; (2) larger UV and emission-line surveys to enlarge sample sizes; and (3) IR spectroscopy (e.g., MOSDEF) to investigate the redshift evolution of the burstiness from higher redshifts.

We thank the anonymous referee for the valuable and constructive comments, which improve this article. Y.G., S.M.F., D.C.K., G.B., and H.Y. acknowledge support from NSF Grant AST-0808133. Support for Program *HST*-GO-12060 and *HST*-AR-13891 were provided by NASA through a grant from the Space Telescope Science Institute, operated by the Association of Universities for Research in Astronomy, Incorporated, under NASA contract NAS5-26555. MR acknowledges support from an appointment to the NASA Postdoctoral Program at Goddard Space Flight Center.

Facilities: *HST* (WFC3), Keck (DEIMOS).

REFERENCES

- Andrews, J. E., Calzetti, D., Chandar, R., et al. 2013, *ApJ*, 767, 51
 Andrews, J. E., Calzetti, D., Chandar, R., et al. 2014, *ApJ*, 793, 4
 Barro, G., Faber, S. M., Pérez-González, P. G., et al. 2013, *ApJ*, 765, 104
 Barro, G., Pérez-González, P. G., Gallego, J., et al. 2011, *ApJS*, 193, 30
 Behroozi, P. S., Wechsler, R. H., & Conroy, C. 2013, *ApJ*, 770, 57
 Bell, E. F., & de Jong, R. S. 2001, *ApJ*, 550, 212
 Boselli, A., Boissier, S., Cortese, L., et al. 2009, *ApJ*, 706, 1527
 Brammer, G. B., van Dokkum, P. G., Franx, M., et al. 2012, *ApJS*, 200, 13
 Bruzual, G., & Charlot, S. 2003, *MNRAS*, 344, 1000
 Calzetti, D., Armus, L., Bohlin, R. C., et al. 2000, *ApJ*, 533, 682
 Cardelli, J. A., Clayton, G. C., & Mathis, J. S. 1989, *ApJ*, 345, 245
 Castellano, M., Sommariva, V., Fontana, A., et al. 2014, *A&A*, 566, A19
 Cerviño, M. 2013, *NewAR*, 57, 123
 Cerviño, M., & Luridiana, V. 2004, *A&A*, 413, 145
 Cerviño, M., & Valls-Gabaud, D. 2003, *MNRAS*, 338, 481
 Chabrier, G. 2003, *PASP*, 115, 763
 Cowie, L. L., & Barger, A. J. 2008, *ApJ*, 686, 72
 da Silva, R. L., Fumagalli, M., & Krumholz, M. 2012, *ApJ*, 745, 145
 da Silva, R. L., Fumagalli, M., & Krumholz, M. R. 2014, *MNRAS*, 444, 3275
 de Barros, S., Reddy, N., & Shivaei, I. 2016, *ApJ*, 824, 81D
 Dekel, A., Birnboim, Y., Engel, G., et al. 2009, *Natur*, 457, 451
 Domínguez, A., Siana, B., Brooks, A. M., et al. 2015, *MNRAS*, 451, 839
 Domínguez, A., Siana, B., Henry, A. L., et al. 2013, *ApJ*, 763, 145
 Eldridge, J. J. 2012, *MNRAS*, 422, 794
 Fall, S. M., & Chandar, R. 2012, *ApJ*, 752, 96
 Forbes, J. C., Krumholz, M. R., Burkert, A., & Dekel, A. 2014, *MNRAS*, 443, 168
 Fumagalli, M., da Silva, R. L., & Krumholz, M. R. 2011, *ApJL*, 741, L26
 Galametz, A., Grazian, A., Fontana, A., et al. 2013, *ApJS*, 206, 10
 Gordon, K. D., Clayton, G. C., Misselt, K. A., Landolt, A. U., & Wolff, M. J. 2003, *ApJ*, 594, 279
 Grogin, N. A., Kocevski, D. D., Faber, S. M., et al. 2011, *ApJS*, 197, 35
 Guo, Y., Ferguson, H. C., Giavalisco, M., et al. 2013, *ApJS*, 207, 24
 Guo, Y., Koo, D. C., Lu, Y., et al. 2016, *ApJ*, 822, 103
 Harris, J., & Zaritsky, D. 2009, *AJ*, 138, 1243
 Henry, A., Martin, C. L., Finlator, K., & Dressler, A. 2013, *ApJ*, 769, 148
 Hopkins, P. F., Kereš, D., Oñorbe, J., et al. 2014, *MNRAS*, 445, 581
 Iglesias-Páramo, J., Boselli, A., Gavazzi, G., & Zaccardo, A. 2004, *A&A*, 421, 887
 Johnson, L. C., Seth, A. C., Dalcanton, J. J., et al. 2016, *ApJ*, 827, 33
 Kennicutt, R. C., & Evans, N. J. 2012, *ARA&A*, 50, 531
 Kennicutt, R. C., Jr. 1998, *ARA&A*, 36, 189
 Koekemoer, A. M., Faber, S. M., Ferguson, H. C., et al. 2011, *ApJS*, 197, 36
 Kriek, M., van Dokkum, P. G., Labbé, I., et al. 2009, *ApJ*, 700, 221
 Krumholz, M. R. 2014, *PhR*, 539, 49
 Krumholz, M. R., Fumagalli, M., da Silva, R. L., Rendahl, T., & Parra, J. 2015, *MNRAS*, 452, 1447
 Kurczynski, P., Gawiser, E., Acquaviva, V., et al. 2016, *ApJL*, 820, L1
 Lada, C. J., & Lada, E. A. 2003, *ARA&A*, 41, 57
 Lee, J. C., Gil de Paz, A., Tremonti, C., et al. 2009, *ApJ*, 706, 599
 Meurer, G. R., Wong, O. I., Kim, J. H., et al. 2009, *ApJ*, 695, 765
 Oke, J. B. 1974, *ApJS*, 27, 21
 Pflamm-Altenburg, J., González-Lópezlira, R. A., & Kroupa, P. 2013, *MNRAS*, 435, 2604
 Pflamm-Altenburg, J., Weidner, C., & Kroupa, P. 2007, *ApJ*, 671, 1550
 Pflamm-Altenburg, J., Weidner, C., & Kroupa, P. 2009, *MNRAS*, 395, 394
 Rafelski, M., Teplitz, H. I., Gardner, J. P., et al. 2015, *AJ*, 150, 31
 Reddy, N. A., Erb, D. K., Pettini, M., Steidel, C. C., & Shapley, A. E. 2010, *ApJ*, 712, 1070
 Reddy, N. A., Kriek, M., Shapley, A. E., et al. 2015, *ApJ*, 806, 259
 Reddy, N. A., Steidel, C. C., Pettini, M., & Bogosavljevic, M. 2016, *ApJ*, 828, 107
 Reines, A. E., Nidever, D. L., Whelan, D. G., & Johnson, K. E. 2010, *ApJ*, 708, 26
 Rutkowski, M. J., Scarlata, C., Haardt, F., et al. 2016, *ApJ*, 819, 81
 Santini, P., Ferguson, H. C., Fontana, A., et al. 2015, *ApJ*, 801, 97
 Searle, L., Sargent, W. L. W., & Bagnuolo, W. G. 1973, *ApJ*, 179, 427
 Shen, S., Madau, P., Conroy, C., Governato, F., & Mayer, L. 2014, *ApJ*, 792, 99
 Shivaei, I., Kriek, M., Reddy, N. A., et al. 2016, *ApJL*, 820, L23
 Shivaei, I., Reddy, N. A., Shapley, A. E., et al. 2015, *ApJ*, 815, 98
 Siana, B., Teplitz, H. I., Colbert, J., et al. 2007, *ApJ*, 668, 62
 Siana, B., Teplitz, H. I., Ferguson, H. C., et al. 2010, *ApJ*, 723, 241
 Sparre, M., Hayward, C. C., Feldmann, R., et al. 2016, *MNRAS*, 464, in press
 Sullivan, M., Treyer, M. A., Ellis, R. S., et al. 2000, *MNRAS*, 312, 442
 Trump, J. R., Konidakis, N. P., Barro, G., et al. 2013, *ApJL*, 763, L6
 Weidner, C., & Kroupa, P. 2005, *ApJ*, 625, 754
 Weidner, C., & Kroupa, P. 2006, *MNRAS*, 365, 1333
 Weidner, C., Kroupa, P., & Pflamm-Altenburg, J. 2011, *MNRAS*, 412, 979
 Weidner, C., Kroupa, P., & Pflamm-Altenburg, J. 2014, *MNRAS*, 441, 3348
 Weisz, D. R., Johnson, B. D., Johnson, L. C., et al. 2012, *ApJ*, 744, 44
 Whitaker, K. E., Franx, M., Leja, J., et al. 2014, *ApJ*, 795, 104
 Wild, V., Charlot, S., Brinchmann, J., et al. 2011, *MNRAS*, 417, 1760
 Wirth, G. D., Willmer, C. N. A., Amico, P., et al. 2004, *AJ*, 127, 3121
 Wuyts, S., Förster Schreiber, N. M., Nelson, E. J., et al. 2013, *ApJ*, 779, 135
 Zahid, H. J., Kewley, L. J., & Bresolin, F. 2011, *ApJ*, 730, 137
 Zeimann, G. R., Ciardullo, R., Gebhardt, H., et al. 2014, *ApJ*, 790, 113